On the Failure Initiation in the Proximal Human Femur Under Simulated Sideways Fall

Originally published in:
Annals of Biomedical Engineering 46(2), https://doi.org/10.1007/s10439-017-1952-z

Funding acknowledgement:
144435 - What predisposes a hip to fracture? (SNF)

Annals of Biomedical Engineering, Vol. 34, No. 3, September 2018 *(© 2018)* pp. 270–283
https://doi.org/10.1007/s10439-017-1952-z

On the Failure Initiation in the Proximal Human Femur Under Simulated Sideways Fall

HASSAN BAHALOO,[1,2] W. S. ENNS-BRAY,[2] I. FLEPS,[2] O. ARIZA,[2,3,4,5] S. GILCHRIST,[3,4,5] R. WIDMER SOYKA,[2] P. GUY,[4,6] H. PALSSON,[1] S. J. FERGUSON,[2] P. A. CRIPTON,[3,4,5,6] and B. HELGASON[2,7]

[1]Faculty of Industrial Engineering, Mechanical Engineering and Computer Science, School of Engineering and Natural Sciences, University of Iceland, Reykjavik, Iceland; [2]Institute for Biomechanics, ETH-Zürich, Zurich, Switzerland; [3]Orthopaedic and Injury Biomechanics Group, University of British Columbia, Vancouver, Canada; [4]Centre for Hip Health and Mobility, University of British Columbia, Vancouver, Canada; [5]Department of Mechanical Engineering, University of British Columbia, Vancouver, Canada; [6]Department of Orthopedics, University of British Columbia, Vancouver, Canada; and [7]School of Science and Engineering, Reykjavik University, Reykjavik, Iceland

(Received 26 June 2017; accepted 30 October 2017; published online 27 November 2017)

Associate Editor Eiji Tanaka oversaw the review of this article.

Abstract—The limitations of areal bone mineral density measurements for identifying at-risk individuals have led to the development of alternative screening methods for hip fracture risk including the use of geometrical measurements from the proximal femur and subject specific finite element analysis (FEA) for predicting femoral strength, based on quantitative CT data (qCT). However, these methods need more development to gain widespread clinical applications. This study had three aims: To investigate whether proximal femur geometrical parameters correlate with obtained femur peak force during the impact testing; to examine whether or not failure of the proximal femur initiates in the cancellous (trabecular) bone; and finally, to examine whether or not surface fracture initiates in the places where holes perforate the cortex of the proximal femur. We found that cortical thickness around the trochanteric-fossa is significantly correlated to the peak force obtained from simulated sideways falling ($R^2 = 0.69$) more so than femoral neck cortical thickness ($R^2 = 0.15$). Dynamic macro level FE simulations predicted that fracture generally initiates in the cancellous bone compartments. Moreover, our micro level FEA results indicated that surface holes may be involved in primary failure events.

Keywords—Proximal femur, Sideways falling, Finite element method, Holes, Trochanteric-fossa cortical shell thickness, Fracture.

Address correspondence to Hassan Bahaloo, Faculty of Industrial Engineering, Mechanical Engineering and Computer Science, School of Engineering and Natural Sciences, University of Iceland, Reykjavik, Iceland. Electronic mail: hassan.bahaloohoreh@hest.ethz.ch

INTRODUCTION

Presently, areal bone mineral density (aBMD) is the clinical "gold standard" used to diagnose osteoporosis (aBMD T-score ≤ −2.5). Although low aBMD is associated with an increased population based fracture risk, 75–85% of hip fractures occur in people without osteoporosis.[47,48,55] The limitations of aBMD measurements for identifying at-risk individuals have led to alternative methods for screening for hip fracture risk being proposed, including the use of geometrical measurements from the proximal femur[14,44,49] and subject specific finite element analysis (FEA) for predicting femoral strength,[2,5,13,21,30–33,35,36,41,42,45,46,52] based on Quantitative CT data (QCT). However, even though QCT-based FE analysis has been demonstrated to be superior to aBMD measurements in terms of predicting *in vitro* measure strength,[27] it is only been demonstrated to be marginally more sensitive in terms of identifying individuals at risk of sustaining a hip fracture when validated against cohort data.[31,42] This could potentially be due to lack of biofidelity of the models with respect to modelling the rate dependency and dynamics of the events that lead to most of the fractures i.e., fall to the side from standing height.[42]

The biomechanics of hip fracture has been studied by many authors in the past. Predictions of the fracture location and character remain speculative, but are believed to be the result of local thinning of the cortex.[4,37,38,50] Several other studies have focused on other geometrical parameters as predictors of hip or vertebral fracture risk, including hip axis length,[14]

vertebral bone width[49] and angle between femoral neck and shaft.[44] The femoral neck has been the focus of attention in many studies,[4,6,15,25,26,37,38] however, some epidemiological studies indicate inter-trochanteric fractures have a comparably frequent occurrence.[10,39]

The link between cancellous structure in the proximal femur and organ-level bone strength is still debated, with some researchers reporting that cancellous bone plays a large role,[6,37,50] while others have found that its role is almost negligible.[4,38] The actual fracture initiation and progression within the proximal femur are not well understood, with some studies providing evidence that fracture of the proximal femur initiates in the cancellous bone,[41] while other studies argue that fracture initiates in the cortical bone.[28,32,54] The role of the vascular architecture of the proximal femur on fracture resistance has not been thoroughly investigated in the literature, but the holes in the cortical shell, through which the vascular structure penetrates, have been suggested as potential fracture initiation sites[23] under para-physiological loading.

There is ample evidence showing that the majority (> 90%) of hip fractures are associated with a short, low trauma fall, and while falls in older adults are common,[20] only 1–5% of the falls result in a fracture,[9,51] with falls to the side producing a high fracture rate.[43] Hip fractures following a side-ways fall are known to be the results of dynamic events in which the strain rate effects become pronounced.[7,18,22] In this context, it is worth noting that evidence from direct mechanical testing of human cortical bone samples indicate that ultimate stress and strain in tension decreases with increasing strain rate while the opposite is the case for cortical bone tested in compression.[22] In addition, it is well established that the failure mechanisms of cellular materials like bone,[16,17,34] under dynamic loading is quite different from that of the quasi static loading.[1,53,54,56] This means that fracture patterns in the proximal femur resulting from quasi-static mechanical testing could be different from fracture patterns resulting from testing of such specimens using realistic impact speeds. This suggests that a more realistic impact model is required to accurately simulate failure mechanisms of the proximal femur in the context of understanding hip fracture risk.

The overall purpose of the present study was to investigate fracture initiation patterns of human femoral specimens subjected to impact loading at speeds representative for side-ways falls on the hip from standing height. The study aims were threefold: First, to correlate the cortical thickness of the trochanteric-fossa and mid-femoral neck with the peak force obtained from dynamic testing. Second, to evaluate whether the hypothesis that failure of the proximal femur initiates in the cancellous bone is supported by evidence from macro level FE simulations, Xtreme CT data, and HS video data gathered from impact tests. Third, to use micro level FE simulations to examine whether holes perforating the proximal femur cortical shell could play a role in surface fracture initiation.

MATERIALS AND METHODS

Experimental Procedure

Data from a previous drop-tower experiment carried out on 15 human donor femurs was used in the present study.[19] A brief description of the protocol is included here for clarity and completeness. Prior to testing, the specimens were scanned in an Xtreme CT scanner at a 41 m resolution (Xtreme CT, Scanco, Inc., Switzerland) calibrated with a standardized hydroxyapatite phantom. The data were resampled to clinical-CT resolution (615 μm) before segmentation was carried out in AMIRA (v.5.3, Visage Imaging Inc., San Diego, CA). The specimens were DXA scanned (QDR4500W, Hologic, Bedford, MA) using 4 kg of rice to simulate soft tissue. The results reported in terms of aBMD, T-scores and degree of osteoporosis classification are reported elsewhere.[2] The drop tower testing rig included a 32 kg (for body) and a 2 kg (for pelvic) impact mass dropped from a height of 0.5 m resulting in a target impact velocity of 3 m/s, a 50 N/mm pelvis spring to simulate pelvic compliance, and 19 mm of closed cell foam covering the greater trochanter to account for the effects of soft tissue.[2] The simulated fall was recorded by four HS video cameras. Two cameras (Phantom V12.1) observed the anterior–superior femoral neck at 10,000 fps (1024 × 800 px, 15 px/mm) for DIC measurement. One camera (Phantom V9) recorded the impact hammer and lateral trochanter at 9216 fps (576 × 288 px, 5 px/mm) for trochanter displacement measurement, and finally, one camera (Phatom V9) qualitatively observed the posterior of the specimen at 6006 fps 480 × 480 px, various spatial resolutions) for fracture monitoring. Impact forces at the greater trochanter were acquired using a six-axis load cell (Sensor Data M211-11; Sterling Heights, MI, ± 13.34 kN (axial range)) at a sampling of 20 kHz. A sample bone under test conditions is depicted in Fig. 1.

Cortical Shell Thickness Measurements

The CT images at original resolution of 41 μm were used to quantify the cortical shell thickness of the fe-

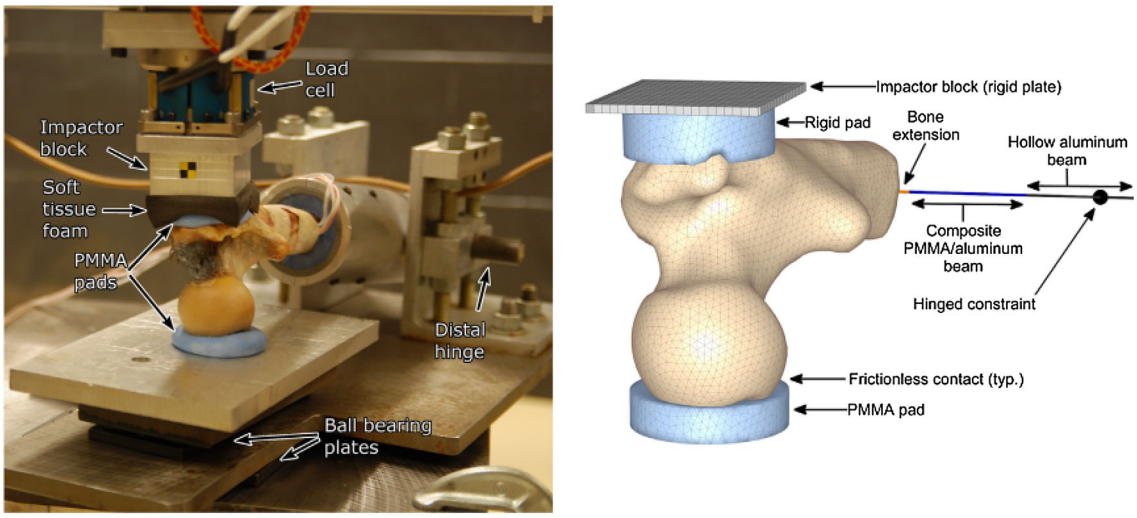

FIGURE 1. Experimental setup drop tower testing (left) and corresponding FE model (right), with rigid plate on which the impact velocity was imposed, upper and lower PMMA pads, beam elements representing distal potting in aluminum, and distal pin constraint. Reprinted from Ariza *et al.*,[2] permission to reprint will be acquired from Elsevier in case the manuscript is accepted for publication.

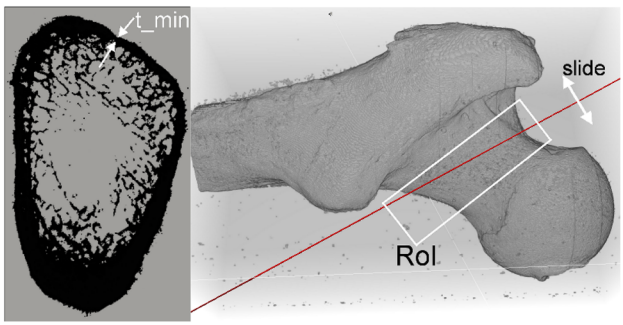

FIGURE 2. Minimum cortical thickness (*t*) measurement in the femoral neck region of interest (RoI) illustrated on a sample specimen.

mur in the trochanteric-fossa and mid-neck regions. The minimum cortical shell thickness in both the superior part of the mid-neck (depicted in Fig. 2, mid-neck is defined as the minimum cross-sectional area of the femoral neck) and trochanteric-fossa region (a cross section parallel to the femoral shaft passing through the trochanteric fossa cavity as shown in Fig. 3) were measured using Paraview (v.4.4, Kitware Inc., New York, NY) and correlated with experimentally measured peak force. To ensure catching the minimum thickness, the cross-sectional planes were translated along an axis normal to the plane, in increments of 1 mm in each direction (Figs. 2 and 3), and five slices were used for each measurement. DXA derived measurements (femoral neck aBMD, trochanteric aBMD and total aBMD) were also correlated with experimentally measured peak force. Pearson's coefficient (R^2) was used to evaluate the proportion variance of the dependent variables (peak force) explained by the variance of the independent variables (aBMD and cortical thickness).

Macro Level Finite Element Analysis

The macro level FEA was originally performed in the study by Enns-Bray *et al.*[12] and reported the simulated force–time and force–displacement in terms of then whole bone. The macro level FEA methodology is briefly explained here for clarity. The FE models (Fig. 1) were constructed based on segmentation of CT data resampled to a 615 μm isotropic spatial resolution. The results from case II in the study of Enns-Bray *et al.*[12] were used in the present study, in which the PMMA cup that supports the femoral head was assumed to be bonded to the ground but the femoral head still allowed to slide freely against the PMMA cup surface. The speed of the impact on greater trochanter derived from the HS video data was used to drive the models to simulate the impact generated by the falling mass. The models were solved in a commercial FE solver (LS-Dyna R7.1.3, Livermore Software Technology Corporation, Livermore CA). The detailed material mapping strategy can be found in Appendix B.

Extended FEA Analysis

In the present study, a semi-automated damage detection algorithm was developed in Paraview that

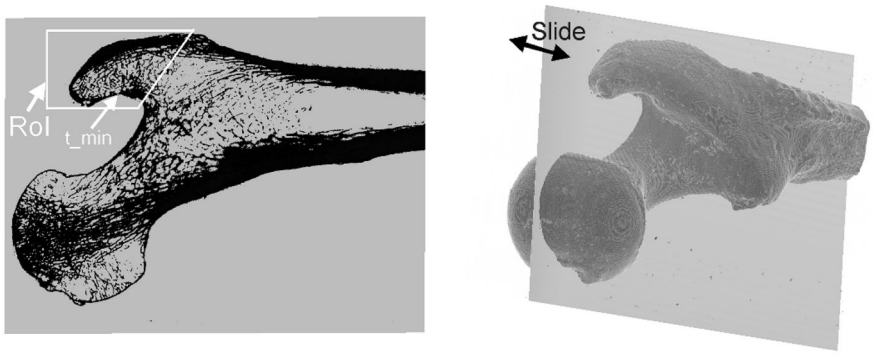

FIGURE 3. Minimum cortical shell thickness (*t*) measurement in the trochanteric-fossa region of interest (RoI) illustrated on a sample specimen.

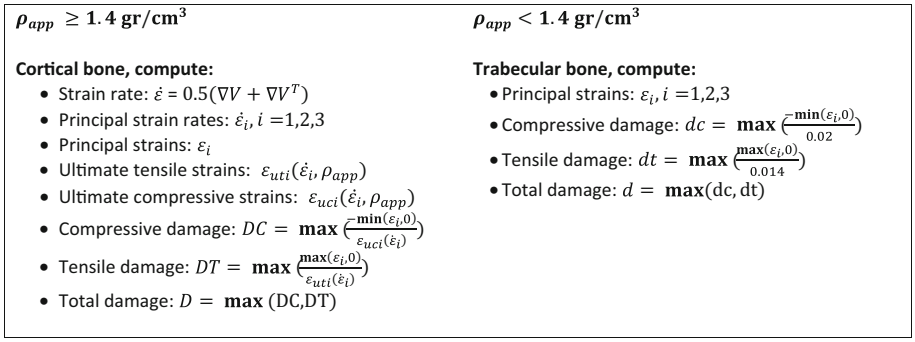

FIGURE 4. The damage detection algorithm implemented in Paraview.

tracked element principal strain at each time step of the simulation and flagged the elements with principal strains above a specified failure threshold. The failure thresholds are indicated in Fig. B1, and pseudo code for the algorithm is provided in Fig. 4. The elements were categorized based on their density as either "Cortical" or "Cancellous" in Paraview. Then the strain rate each at elements was calculated in Paraview using the nodal velocity outputs from LS-DYNA. The ultimate compressive & tensile strains were defined for each element as functions of density and strain rate based on cortical and cancellous formulations according to the material mapping strategy (Appendix B). A damage parameter was defined as the ratio of the principal compressive/tensile strain to the corresponding ultimate compressive/tensile strain at each element. Finally, using the "Find Data" filter in Paraview, the elements with damage parameter greater than 1 were flagged as failed elements.

In the present study, the damage detection algorithm was used to examine systematically whether observations from macro level FEA results support the hypothesis that failure initiates in the cancellous bone compartments and not on the cortical surface. The locations of the first failed elements according to macro level FE simulations are indicated as SIM0 in Fig. 5. If the first failing element in the simulation was not a surface element, then the progression of failing elements was tracked through the simulation time steps until the first surface element failed according to the damage detection algorithm, indicated with SIM1 in Fig. 5. The location and time of the first crack appearing on the surface of the bones according to the high-speed video data is indicated with EXP1 in Fig. 5. The location and time of SIM1 and EXP1 was subsequently compared. An example of the outcome of this type of analysis provided for a single specimen in Fig. 5 with complete results from the analysis for all the specimens is provided as supplementary material.

Micro Level Finite Element Analysis

To test the hypothesis that holes perforating the cortical shell are associated with primary failure events under experimentally simulated sideways fall impact, micro level FE analysis was carried out using the protocol described in Helgason *et al.*[23] for 3 selected femurs, each of them representing one out of 3 main failure types according to previous results[2] (H1167L: intertrochanteric failure, H1366R: head-neck junction

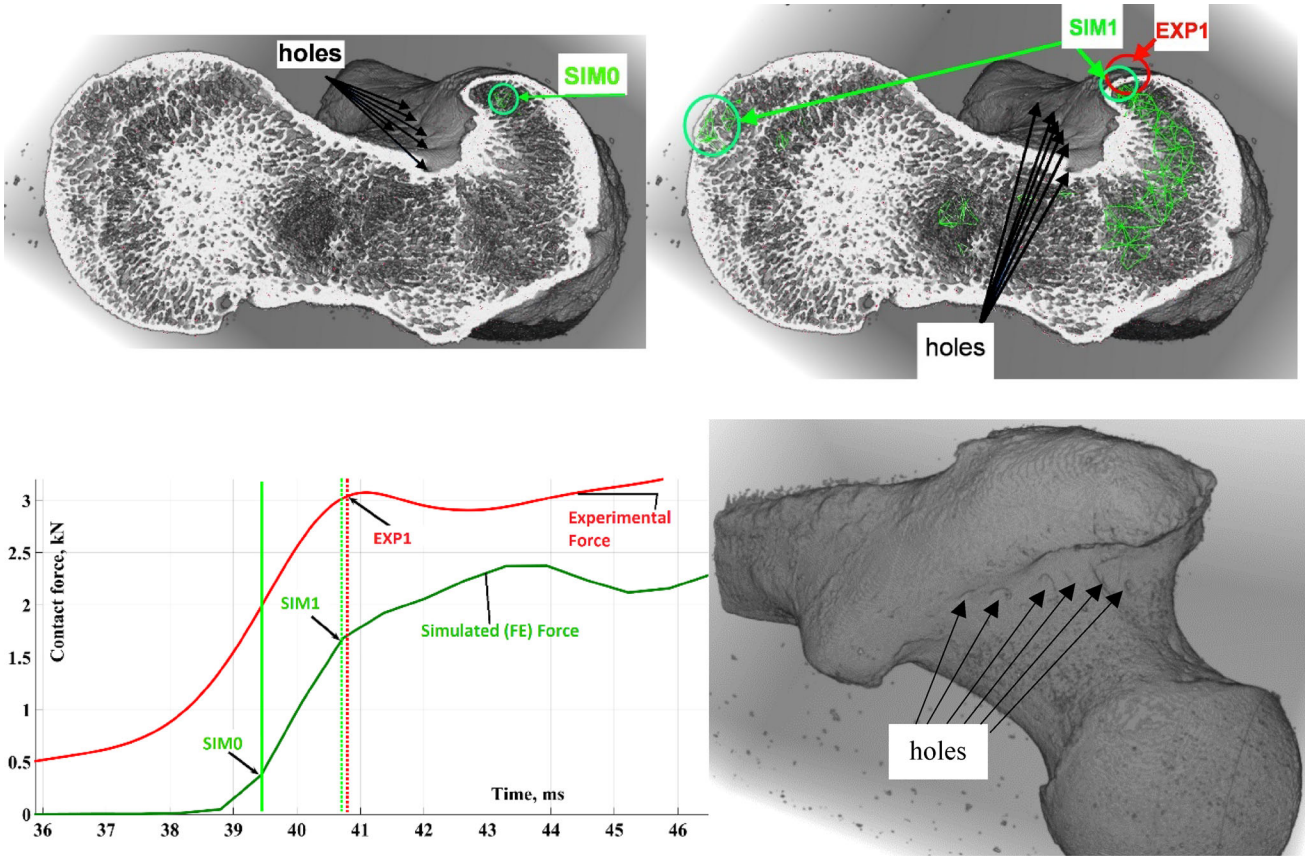

FIGURE 5. Failure locations according to experimental results and FEA; (top left) SIM0: first failing element based on FEA at $t = 39.44$ ms; (top right) EXP1: first failure observed on the bone surface according to HS video image data at $t = 40.88$ ms; SIM1: first failing surface element based on macro level FEA at $t = 40.73$; (bottom left) plot of impact force at the Greater Trochanter (GT) with failure events indicated; (bottom right) zoomed view of the holes.

failure, H1375L: basi-cervical failure). In the present study, a $8 \times 8 \times 8$ mm^3 volume of interest (VOI) was defined centered around the location of first crack visible on the surface of the bones according to the HS video data which is the location previously defined as EXP1. In the interest of reducing computational time and allowing for larger VOIs being studied than in the work of Helgason *et al.*[23] the high resolution stack was rescaled to 82 μm resolution and each bone voxel translated to a 8-node hexahedral finite element. As in the work of Helgason *et al.*,[23] material properties were mapped to the hexahedral elements of the micro level models based on the gray level of the voxels using the same material card as was used in the macro level FEA of the bones. The applied boundary conditions were in the form of the cube face velocities whose values were extracted from corresponding macro level FE results. A 3D interpolation scheme using the built-in "TriScatteredInterp" function in Matlab (v.R2016b, The Mathworks, Natick, MA, USA) was used to assign a velocity value from macro (lower) to micro (higher) level resolution on the faces of the cube. 1st and 3rd principal strain patterns were measured in the micro FE cubes, and were qualitatively compared to the observed failure location and pattern during the drop tower experiments. The simulations were conducted on a computer system with 6 Core i7-4930K@3.4GHz Intel CPUs and 32GB of memory. The simulations took between 24 and 48 h depending on the models. The number of elements for specimens H1167L, H1366R, and H1375L were 152,947, 74,685, and 328,893 respectively.

RESULTS

Bone Geometrical Parameters

The cortical shell thickness of the trochanteric-fossa was moderately correlated with measured peak force ($R^2 = 0.69$, $p = 0.0001$, Fig. 6a), and there was a small correlation between the minimum cortical thickness at the mid-femoral neck and peak force ($R^2 = 0.15$, $p = 0.15$, Fig. 6a). The measured trochanteric aBMD showed a stronger correlation to the measured peak

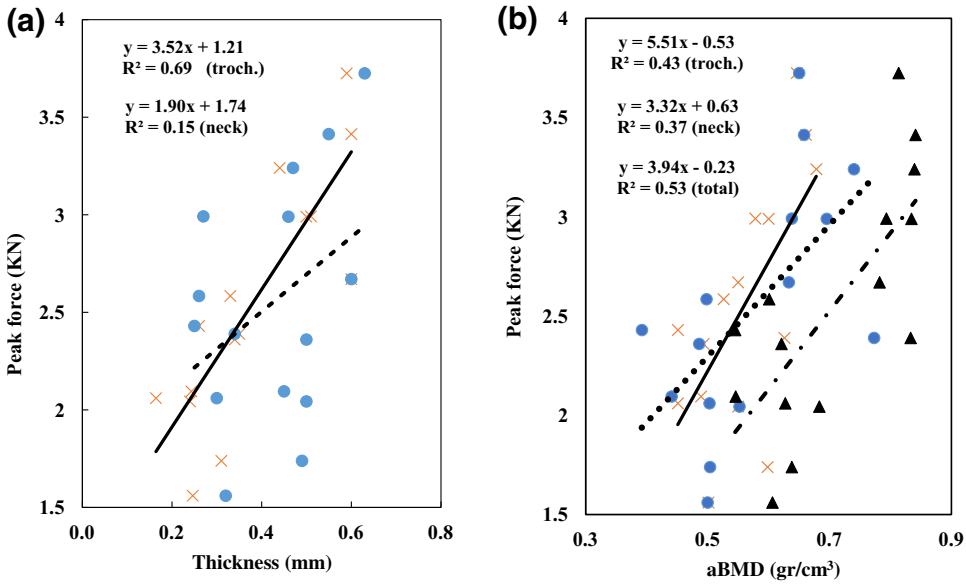

FIGURE 6. (a) Measured peak force vs. femoral shell thickness measured in the femoral neck (circle) and the greater trochanter (×); (b) Measured peak force vs. aBMD measured at the neck (circle), greater trochanter (×) and total aBMD (triangle).

TABLE 1. Damage Initiation sites in the human femoral specimens.

Specimen	SIM0	Is SIM0 internal?	SIM1 vs. EXP1 location agreement
H1167L	Troch.	Yes	Yes
H1168R	Subcervical	Yes	Yes
H1365R	Troch.	Yes	Yes
H1366R	Troch., neck–head	Yes	Yes
H1368R	Head	Yes	No
H1369L	Troch.	Yes	No
H1372R	Troch./Head	Yes	No
H1373R	Troch.	Yes	No
H1374R	Head	Yes	Yes
H1375L	Troch.	Yes	Yes
H1376L	Troch.	Yes	Yes
H1377R	Troch.	Yes	Yes
H1380R	Head	No	No
H1381R	Head	Yes	No
H1382L	Troch.	Yes	No

force than femoral neck aBMD ($R^2 = 0.43$, $p = 0.0016$, and $R^2 = 0.37$, $p \ll 0.008$, respectively, Fig. 6b). The correlation between the total bone aBMD and the measured peak force was greater than both trochanteric and neck correlations ($R^2 = 0.53$, $p = 0.002$, Fig. 6b).

Macro Level FEA

Damage initiation sites based on the simulation results are presented in Table 1. From these results, it is evident that the greater trochanter and femoral head regions are the most dominant regions in term of damage initiation. Furthermore, according to the organ level simulations, the damage initiates in the cancellous bone compartments for all specimens except for one bone (H1380R), in which damage initiates simultaneously in the cancellous bone and on the surface of the femoral head area making it difficult to identify firmly from which location the damage first initiates.

Agreement between first visible crack according to HS video data (EXP1), and first surface element failing according to macro level FEA (SIM1) was found for 8 out of the 15 specimens. In 5 out of 7 bones that the predicted (SIM1) and observed (EXP1) crack locations do not match, crack is located in greater trochanter region based on the observations. This suggests that the material mapping in the study with Enns-Bray *et al.*[12] to be modified to consider separate material mapping strategies for neck and trochanteric regions,

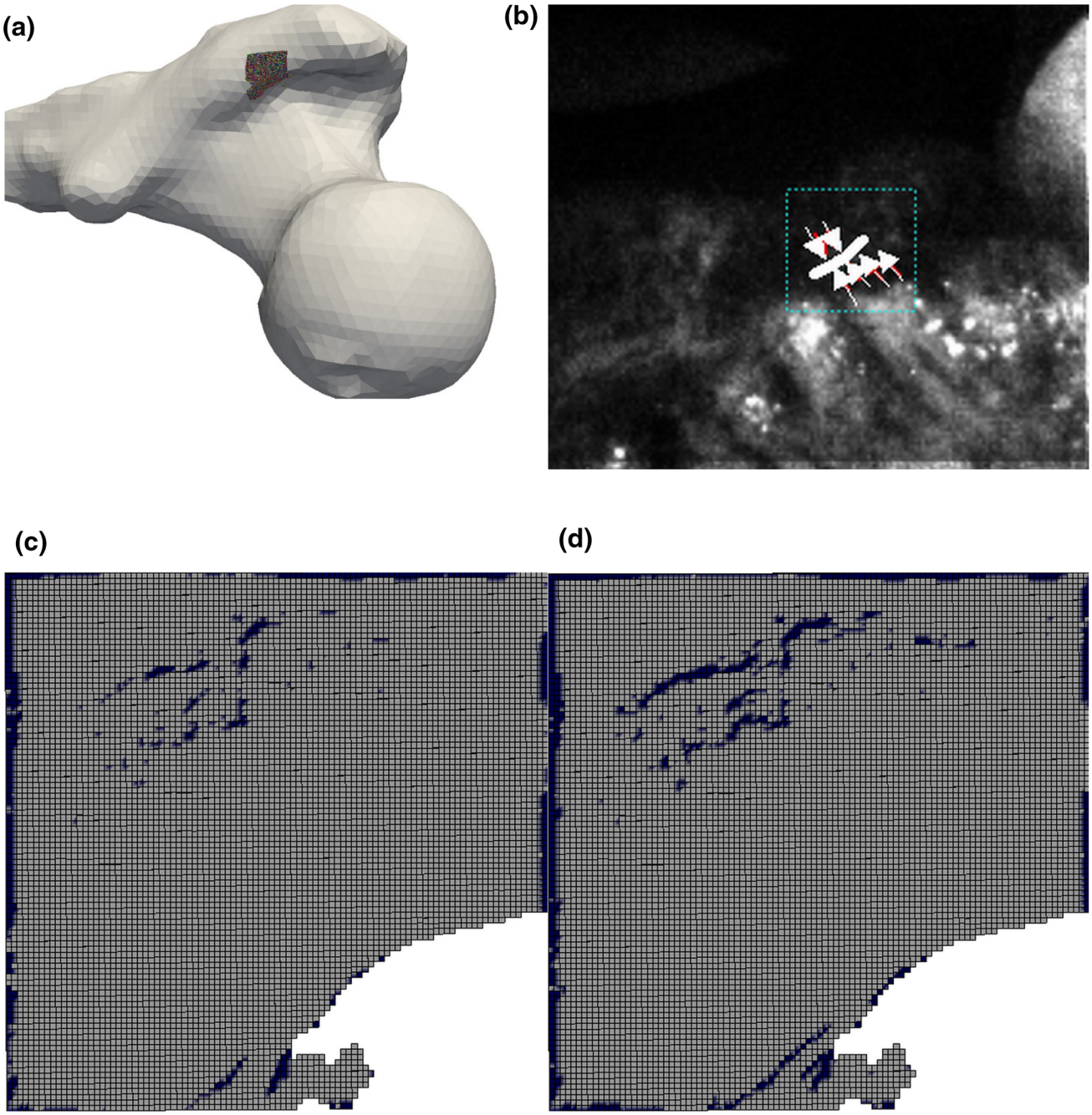

FIGURE 7. Micro FE simulations for bone H1167L (a) the selected cube for micro FE simulations shown on macro level FE; (b) fracture site observed in HS video; (c, d) micro FE simulation result for elements undergoing tensile failure. (a) Selected VOI, (b) 40.878 ms, (c) 38.4 ms, (d) 40.4 ms.

specifically a material mapping with lower ultimate strain for trochanteric region.

Micro Level FEA

The micro level FEA results of the three selected femoral specimens are illustrated in Figs. 7, 8, and 9. For specimen H1167L, tensile failure was observed with no elements failing in compression. For the second selected bone (H1366R), both compressive and tensile failure modes were present at initial failure location (Fig. 8). This is in accordance with the folding behavior of the surface, which was observed from the HS videos (Fig. 8b). Elements in the third selected bone (H1375L) failed exclusively in compression (Fig. 9).

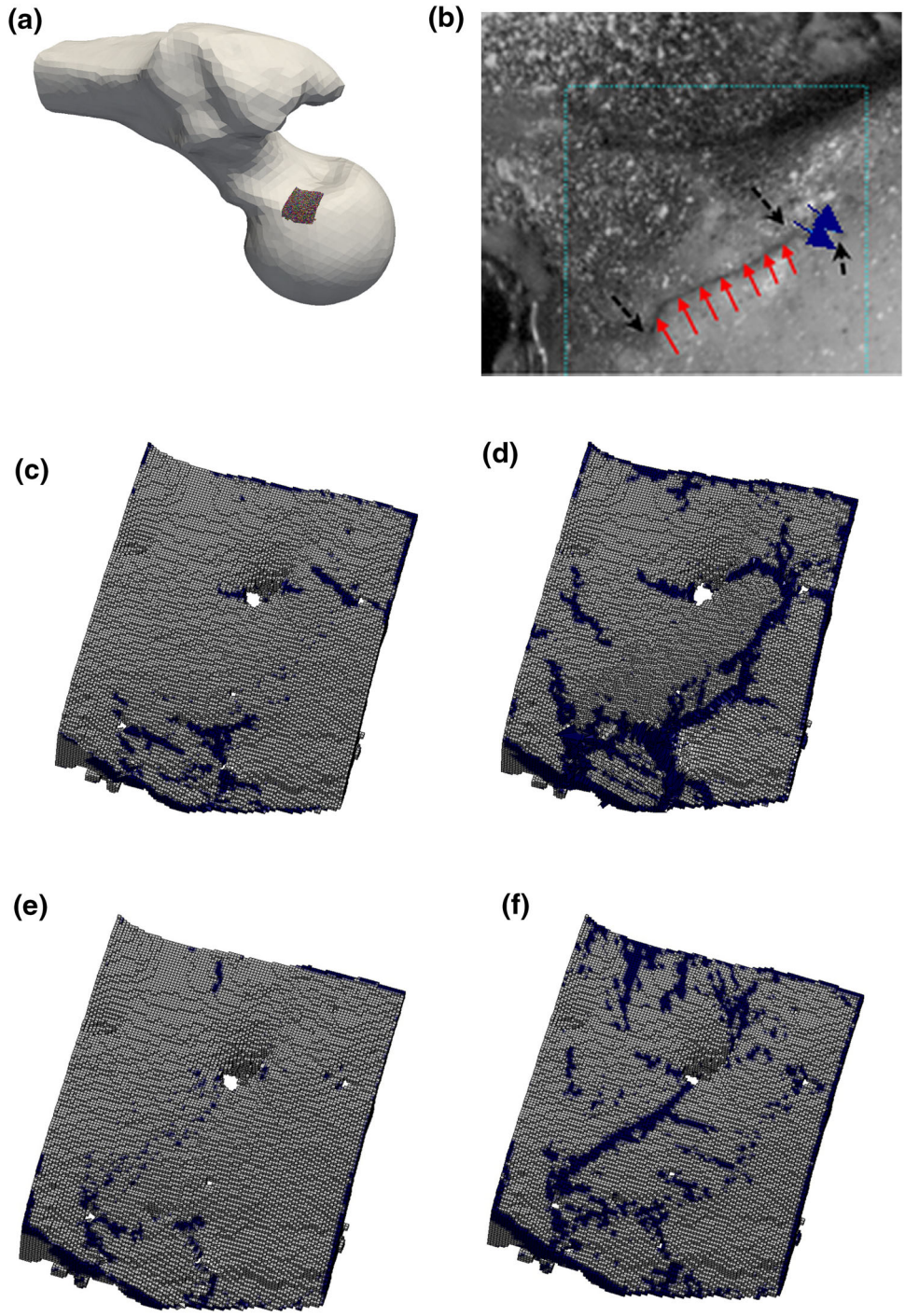

FIGURE 8. Micro FE simulations for bone H1366R (a) the selected cube for micro FE simulations shown on macro level FE. (b) fracture site observed in HS video (arrows, each blue and red shows two different observable crack paths) and the hole location (dashed arrows); (c, d) micro FE simulation result for elements undergoing tensile failure; (e, f) micro FE simulation result for elements undergoing compressive failure. (a) Selected VOI, (b) 37.9 ms, (c) 34.9 ms, (d) 37.1 ms, (e) 34.9 ms, (f) 37.1 ms.

For two of the selected specimens (H1366R, H1375L) the initial surface failure events (EXP1) were related to the holes perforating the cortex. High strain concentrations were observed in micro level FE analyses near the holes for these. The surface failure in specimen H1366R is particular since the strain pattern according to the micro level FEA expresses two main lines of high strains. Careful study of the HS video data around the time of failure supports this by revealing a folding plate from cortical shell portion of

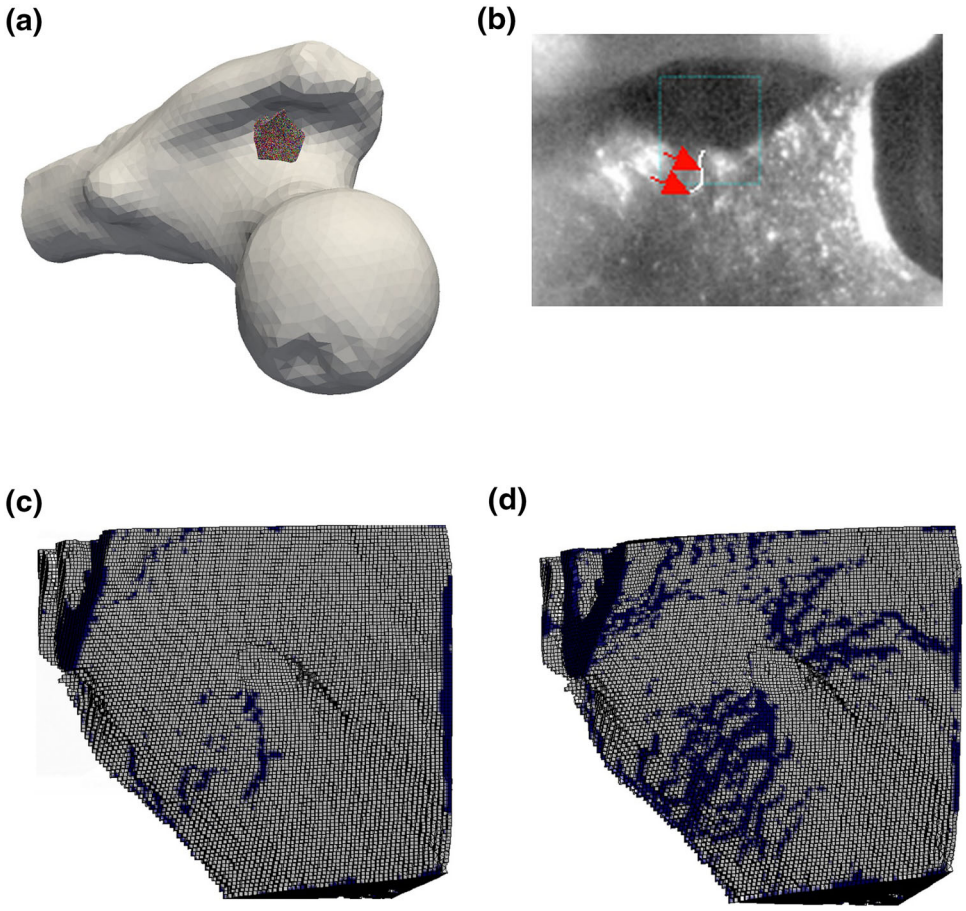

FIGURE 9. Micro FE simulations for bone H1375L (a) the selected cube for micro FE simulations shown on macro level FE; (b) fracture site observed in HS video; (c, d) micro FE simulation result for elements undergoing compressive failure. (a) Selected VOI, (b) 40.96 ms, (c) 37.6 ms, (d) 40.7 ms.

that region. This folding behavior necessitates one edge of the plane to undergo tension while the other edge undergoes compression.

DISCUSSIONS

This study had three aims: To investigate whether proximal femur geometrical parameters correlate with outcomes of the impact testing; to examine whether or not failure of the proximal femur initiates in the cancellous bone; and finally, to examine whether or not surface fracture initiates in the places where holes perforate the cortex of the proximal femur. We found trochanteric-fossa cortical thickness to be moderate correlated to the peak impact force obtained from simulated sideways falling ($R^2 = 0.69$), more so than femoral neck cortical thickness ($R^2 = 0.15$). Dynamic macro level FE simulations predicted that fracture generally initiates in the cancellous bone compartments. Moreover, our micro level FEA results indicated that surface holes can be involved in primary failure events.

Previous studies have examined the relationship between neck shell thinning and risk of fracture,[4,6,15,25,26,37,38] however, to the best of the authors' knowledge, there has been no previous study comparing the trochanteric cortical shell thickness to the failure load of the femur. Our results indicated that trochanteric-fossa cortical shell thickness is better correlated with measured peak force than the mid-neck cortical shell thickness ($R^2 = 0.69$ vs. $R^2 = 0.15$,) and better correlated with peak force than the three aBMD measurements ($R^2 = 0.43$, $R^2 = 0.37$ and $R^2 = 0.53$). These results indicate that under impact load the fracture initiation site moves closer to the impact site compared to fracture resulted from quasi-static loading. This can be related to the fact that failure mechanisms of cellular materials have different failure patterns under dynamic loading from that of in quasi static loading.[1,16,17,34,54,56] A dimensionless parameter

governing the behavior of materials under impact loading is[53]:

$$\bar{V} = V\sqrt{E\rho}/\sigma_y \quad (1)$$

where V, E, ρ, and σ_y are impact velocity, modulus of elasticity, local density, and initial yield stress respectively. Increasing $\bar{V}$ results in the deformation mode changing from quasi-static to transition and dynamic where local deformations become pronounced.[1,56] Assuming an impact velocity of 3 m/s and using relevant data for the modulus of elasticity and yield stress from our material mapping strategy results in $\bar{V} > 5$ for the low density cancellous bone compartments but this is generally assumed to be indicative of dynamic effects being present.[1]

We found that damage initiated inside the bone for 14 out of 15 femurs according to the macro level FEA results as reported in Table 1. This finding is in line with the study by Nawathe *et al.*[40] where based on micro level FE (82 μm) simulations of the proximal femur concluded that damage always initiates in the cancellous bone due to the lack of structural redundancy. However, our observation is based on macro level FE (615 μm) which is in clinical resolution. For 11 out of 15 femurs, the initial surface damage related to trochanteric failures which is in line with clinical literature reporting high prevalence of intertrochanteric fractures.[29]

We obtained strain patterns using micro FE simulations for the volumes of interest centered on the location where surface fracture is first observed according to HS video data. Holes perforating the cortex were also observed for 2 out of 3 specimens (H13665 and H1375L). Interestingly, the strain patterns and failure mode (tension vs. compression) were at least qualitatively similar to observations from the HS video data, suggesting that this multi-scale technique is a useful tool for analyzing the details of the fracture initiation, even for an event as complex as simulated side-ways fall impact.

Our study contains a number of limitations. First, the numbers of specimens measured or simulated is limited. Second, since the real nature of the material and loading is very complicated, the simplifications and assumptions in making FE models and material mapping can affect the results. "Bone is an anisotropic material and while it has been shown that including anisotropy to the material mapping strategy has little effect on macroscopic measurements such as peak force, it could play a role in local strains."[12] Furthermore, the experimental and simulated boundary conditions would ideally be more biofidelic by including additional neighboring structures such as the distal legs and pelvis, as well as modelling the soft tissue that encapsulates the femur and determines how much impact energy is distributed over the femur instead of transferring the load to the femur *via* displacement of a PMMA cup. Third, even though our data supports the argument that fracture of the proximal femur generally initiates in the cancellous bone compartment, verifying that experimentally is difficult.

In summary, we found evidence suggesting that greater trochanter bone morphology may be relevant for assessing fracture risk of the proximal femur under impact. Furthermore, it is possible that fracture primarily initiates in the cancellous bone compartments before reaching the bone surface, whereby the fracture can propagate from the point of initiation towards locations on the surface were holes (from vascularization or otherwise) perforate the cortical shell. Understanding the localization of femoral fracture could have important implications for future research of fracture prevention.

APPENDIX A

Strain rate dependency functions for cortical bone.

$$\begin{aligned}
\alpha_{u,t}(\dot{\varepsilon}) &= -2.093\times10^{-5}\min(\dot{\varepsilon},18)^3 + 1.420 \\
&\quad \times 10^{-3}\min(\dot{\varepsilon},18)^2 - 5.082\times10^{-2}\min(\dot{\varepsilon},18) + 1 \\
\alpha_{y,t}(\dot{\varepsilon}) &= -1.424\times10^{-5}\min(\dot{\varepsilon},18)^3 + 4.395 \\
&\quad \times 10^{-4}\min(\dot{\varepsilon},18)^2 - 3.466\times10^{-2}\min(\dot{\varepsilon},18) + 1 \\
\beta_{u,t}(\dot{\varepsilon}) &= -3.613\times10^{-6}\min(\dot{\varepsilon},18)^5 + 2.034 \\
&\quad \times 10^{-4}\min(\dot{\varepsilon},18)^4 - 4.501\times10^{-3}\min(\dot{\varepsilon},18)^3 \\
&\quad + 4.967\times10^{-2}\min(\dot{\varepsilon},18)^2 - 0.280\min(\dot{\varepsilon},18) + 1 \\
\beta_{y,u}(\dot{\varepsilon}) &= 9.005\times10^{-6}\min(\dot{\varepsilon},18)^4 - 2.819 \\
&\quad \times 10^{-4}\min(\dot{\varepsilon},18)^3 + 2.626\times10^{-3}\min(\dot{\varepsilon},18)^2 \\
&\quad - 0.039\min(\dot{\varepsilon},18) + 1
\end{aligned} \quad (A1)$$

$$\begin{aligned}
\alpha_{u,c}(\dot{\varepsilon}) &= -1.028\times10^{-3}\min(\dot{\varepsilon},30)^2 + 3.063 \\
&\quad \times 10^{-2}\min(\dot{\varepsilon},30) + 1 \\
\alpha_{y,c}(\dot{\varepsilon}) &= -1.920\times10^{-2}\min(\dot{\varepsilon},30) + 1 \\
\beta_{u,c}(\dot{\varepsilon}) &= -8.830\times10^{-3}\min(\dot{\varepsilon},30)^2 + 0.303\min(\dot{\varepsilon},30) + 1 \\
\beta_{y,c}(\dot{\varepsilon}) &= -2.463\times10^{-2}\min(\dot{\varepsilon},30) + 1
\end{aligned} \quad (A2)$$

APPENDIX B

The material mapping strategy used in the study of Enns-Bray *et al.*[12] simulated the material properties of bone tissue using a crushable Fu Chang foam model (MAT 083, in LS-Dyna),[8] which includes properties such as: strain rate effects and post-yield asymmetry between tension and compression. Ash density was derived from the resampled CT data using the following relationship[2]:

$$\rho_{\text{ash}} = (\text{mgHA}/1000 + 0.09)/1.14\,\text{g/cm}^3 \quad \text{(B1)}$$

Apparent density (ρ_{app}) was defined as

$$\rho_{\text{app}} = \rho_{\text{ash}}/0.6 \quad \text{(B2)}$$

The modulus of elasticity was derived using the modulus–density relationship from Morgan *et al.*[40]

$$E = 6850\rho_{\text{app}}^{1.49} \quad \text{(B3)}$$

Strain rate scaling (SRS) for cancellous bone remained the same as in the previous study[2] (using the equation proposed by Carter and Hayes's[7]).

$$\text{SRS} = (\dot{\varepsilon}/0.005)^{0.06} \quad \text{(B4)}$$

The details of the post yield response are described in Enns-Bray *et al.*,[12] but summarized in Tables B1 and B2.

The proportionality limit, i.e., end of purely elastic deformation, for cortical and cancellous bone ($\sigma_{p,\text{cort}}$, $\sigma_{p,\text{trab}}$) is 80% of the corresponding yield stress.[24] For tensile loading, a damage rule defined as the following exponential is implemented on the stress–strain curve,

$$\sigma_{\text{d}} = \sigma_{u,t}(0.9e^{-25\varepsilon} + 0.1) \quad \text{(B5)}$$

The strain rate effect of the modulus of elasticity for cortical bone was derived based on the data from Hansen *et al.*[22]:

$$E_{\text{C}}^{\text{CO}}(\dot{\varepsilon}) = E(1 + 0.0163\min(\dot{\varepsilon}, 30)) \quad \text{(B6)}$$

$$E_{\text{T}}^{\text{CO}}(\dot{\varepsilon}) = E(1 + 0.0297\min(\dot{\varepsilon}, 18)) \quad \text{(B7)}$$

Examples of full stress–strain curves in tension and compression, for both cancellous ($\rho_{\text{app}} = 1.0$ g/cm^3) and cortical bone ($\rho_{\text{app}} = 1.8$ g/cm^3) are provided in Fig. B1, using the sign convention of LS-Dyna, which assumes positive stress–strain as compression and negative stress–strain as tension.[12]

TABLE B1. Mathematical relationships for describing ultimate stress (σ_u) and yield stress (σ_y) for bone in the macro level FEA. Subscript *t* denotes properties in tension, while subscript *c* denotes prpoperties in compression.

Parameter	Relation	Reference(s)	Remark
$\sigma_{\text{u,c,trab}}$	$49.5 \times SRS \times \rho_{\text{app}}^2$	3, 7	Ultimate stress in cancellous bone
$\sigma_{\text{u,t,trab}}$	$0.7\sigma_{\text{u,c,cort}}$		
$\sigma_{\text{y,c,trab}}$	$\sigma_{\text{u,c,trab}}/1.1$	24	Cancellous yield stress
$\sigma_{\text{y,t,trab}}$	$\sigma_{\text{u,t,trab}}/1.1$		
$\sigma_{\text{u,c,cort}}$	$49.5\rho_{\text{app}}^2\alpha_{\text{u,c}}(\dot{\varepsilon})$	See Appendix A[7,22]	Cortical ultimate stress
$\sigma_{\text{u,t,cort}}$	$33.93\rho_{\text{app}}^2\alpha_{\text{u,t}}(\dot{\varepsilon})$		
$\sigma_{\text{y,c,cort}}$	$37.6\rho_{\text{app}}^2\alpha_{\text{u,c}}(\dot{\varepsilon})$	See Appendix A[7,22]	Cortical yield stress
$\sigma_{\text{y,t,cort}}$	$27.95\rho_{\text{app}}^2\alpha_{\text{u,t}}(\dot{\varepsilon})$		

TABLE B2. Mathematical relationships for describing ultimate strain (ε_u) and yield strain (ε_y) for bone in the macro level FEA. Subscript *t* denotes properties in tension, while subscript *c* denotes prpoperties in compression.

Parameter	Relation	Reference(s)	
$\varepsilon_{\text{u,c,trab}}$	0.02	2	Cancellous ultimate strain
$\varepsilon_{\text{u,t,trab}}$	0.014		
$\varepsilon_{\text{y,c,trab}}$	$0.002 + \sigma_{\text{y,c,trab}}/E$	0.002 offset method	Cancellous yield strain
$\varepsilon_{\text{y,t,trab}}$	$0.002 + \sigma_{\text{y,c,trab}}/E$		
$\varepsilon_{\text{u,c,cort}}$	$0.0164\beta_{\text{u,c}}(\dot{\varepsilon})$	See Appendix A[22]	Cortical ultimate strain
$\varepsilon_{\text{u,t,cort}}$	$0.0276\beta_{\text{u,t}}(\dot{\varepsilon})$		
$\varepsilon_{\text{y,c,cort}}$	$0.0012\beta_{\text{y,c}}(\dot{\varepsilon})$	See Appendix A[22]	Cortical yield strain
$\varepsilon_{\text{y,t,cort}}$	$0.0086\beta_{\text{y,t}}(\dot{\varepsilon})$		

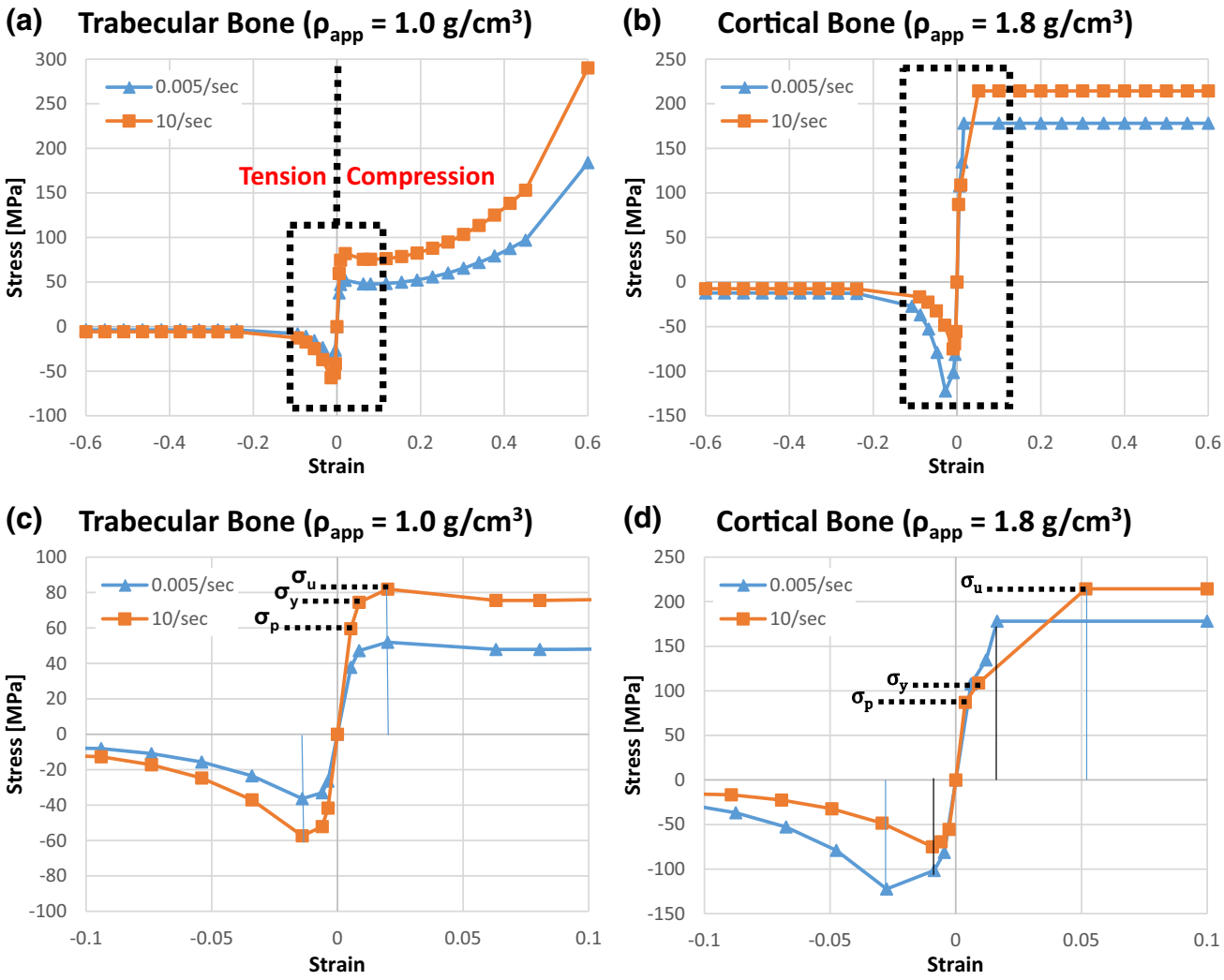

FIGURE B1. Full stress strain curves for cancellous (top left) and cortical bone (top right); windowed regions of full stress strain curve for cancellous (below left) and cortical (below right); showing ultimate stress, yield stress, and proportionality limit for compression (positive) and tension (negative), for high (red) and low (blue) strain rates. The sign convention of LS-Dyna is used which assumes positive stress–strain as compression and negative stress–strain as tension. The failure lines (vertical lines on the stress–strain curves) for both cancellous and cortical bone are indicated based on the ultimate strain failure criteria for compression and tension. Reproduced and modified from Enns-Bray *et al.*[12]

ELECTRONIC SUPPLEMENTARY MATERIAL

The online version of this article (https://doi.org/10.1007/s10439-017-1952-z) contains supplementary material, which is available to authorized users.

ACKNOWLEDGMENTS

This research was supported in part by the St. Josef's Hospital Fund, Reykjavik, Iceland and the Swiss National Science Foundation (Project No. 205321_144435) and the ETH Foundation, Switzerland (Project No. 1514-1).

REFERENCES

[1]Ajdari, A., H. Nayeb-Hashemi, and A. Vaziri. Dynamic crushing and energy absorption of regular, irregular and functionally graded cellular structures. *Int. J. Solids Struct.* 48:506–516, 2011.

[2]Ariza, O., S. Gilchrist, R. P. Widmer, P. Guy, S. J. Ferguson, P. A. Cripton, and B. Helgason. Comparison of explicit finite element and mechanical simulation of the proximal femur during dynamic drop-tower testing. *J. Biomech.* 48:224–232, 2015.

[3]Bayraktar, H. H., E. F. Morgan, G. L. Niebur, G. E. Morris, E. K. Wong, and T. M. Keaveny. Comparison of the elastic and yield properties of human femoral trabecular andcortical bone tissue. *J. Biomech.* 37:27–35, 2004.

[4]Bell, K. L., N. Loveridge, J. Power, N. Garrahan, M. Stanton, M. Lunt, B. F. Meggitt, and J. Reeve. Structure of the femoral neck in hip fracture: cortical bone loss in the inferoanterior to superoposterior axis. *Bone Miner Res.* 14:111–119, 1999.
[5]Bessho, M., I. Ohnishi, T. Matsumoto, S. Ohashi, J. Matsuyama, K. Tobita, M. Kaneko, and K. Nakamura. Prediction of proximal femur strength using a CT-based nonlinear finite element method: differences in predicted fracture load and site with changing load and boundary conditions. *Bone* 45:226–231, 2009.
[6]Black, D. M., M. L. Bouxsein, L. M. Marshall, S. R. Cummings, T. F. Lang, J. A. Cauley, K. E. Ensrud, C. M. Nielson, and E. S. Orwoll. Proximal femoral structure and the prediction of hip fracture in men: a large prospective study using QCT. *J. Bone Miner. Res.* 23(8):1326–1333, 2008.
[7]Carter, D. R., and W. C. Hayes. Epidemiology and outcomes of osteoporotic fractures. *Clin. Orthop. Rel. Res.* 127:265–274, 1977.
[8]Chang, F. S. Constitutive Equation Development of Foam Materials. Ph.D. dissertation, Wayne State 16 University, May 1995.
[9]Cummings, S. R., and L. J. Melton. Epidemiology and outcomes of osteoporotic fractures. *Lancet* 359:1761–1767, 2002.
[10]Desai, K. B., W. J. Ribbans, and G. J. Taylor. Incidence of five common fracture types in an institutional epileptic population. *Injury* 27:97–100, 1996.
[11]Enns-Bray, W. S., O. Ariza, S. Gilchrist, R. W. Soyka, P. J. Vogt, H. Palsson, S. K. Boyd, P. Guy, P. A. Cripton, S. J. Ferguson, and B. Helgason. Morphology based anisotropic finite element models of the proximal femur validated with experimental data. *Med. Eng. Phys.* 38(11):1339–1347, 2016.
[12]Enns-Bray, W. S., H. Bahaloo, I. Fleps, O. Ariza, S. Gilchrist, R. Widmer, P. Guy, H. Palsson, S. J. Ferguson, P. A. Cripton, and B. Helgason. Material mapping strategy to improve the predicted response of the proximal femur to a sideways fall impact. *J. Mech. Behav. Biomed. Mater.* 2017. https://doi.org/10.1016/j.jmbbm.2017.10.033.
[13]Falcinelli, C., E. Schileo, L. Balistreri, F. Baruffaldi, B. Bordini, M. Viceconti, U. Albisinni, F. Ceccarelli, L. Milandri, A. Toni, and F. Taddei. Multiple loading conditions analysis can improve the association between finite element bone strength estimates and proximal femur fractures: a preliminary study in elderly women. *Bone* 67:71–80, 2014.
[14]Faulkner, K. G., S. R. Cummings, M. C. Nevitt, A. Pressman, M. Jergas, and H. K. Genant. Hip axis length and osteoporotic fractures: study of Osteoporotic Fractures Research Group. *J. Bone Miner. Res.* 10:506–508, 1995.
[15]Fox, K. M., S. R. Cummings, E. Williams, and K. Stone. Femoral neck and intertrochanteric fractures have different risk factors. *Osteoporos. Int.* 11:1018–1023, 2000.
[16]Gibson, L. J. The mechanical behavior of cancellous bone. *J. Biomech.* 18(5):317–328, 1985.
[17]Gibson, L. J., M. F. Ashby, and B. A. Harley. Cellular Materials in Nature and Medicine. Cambridge: Cambridge University Press, 2010.
[18]Gilchrist, S., P. Guy, and P. A. Cripto. Development of an inertia-driven model of sideways fall for detailed study of femur fracture mechanics. *J. Biomech. Eng.* 135:121001, 2013.
[19]Gilchrist, S., K. K. Nishiyama, P. DeBakker, P. Guy, S. K. Boyd, T. Oxland, and P. A. Cripton. Proximal femur elastic behavior is the same in impact and constant displacement rate fall simulation. *J. Biomech.* 47(15):3744–3749, 2014.
[20]Graafmans, W. C., M. E. Ooms, H. M. Hofstee, P. D. Bezemer, L. M. Bouter, and P. Lips. Falls in the elderly: a prospective study of risk factors and risk profiles. *Am. J. Epidemiol.* 143:1129–1136, 1996.
[21]Haider, I. T., A. D. Speirs, and H. Frei. Effect of boundary conditions, impact loading and hydraulic stiffening on femoral fracture strength. *J. Biomech.* 46:2115–2121, 2013.
[22]Hansen, U., P. Zioupos, R. Simpson, J. D. Currey, and D. Hynd. The effect of strain rate on the mechanical properties of human cortical bone. *J. Biomech. Eng.* 130:011011, 2008.
[23]Helgason, B., S. Gilchrist, O. Ariza, J. D. Chak, G. Zheng, R. P. Widmer, S. J. Ferguson, P. Guy, and P. A. Cripton. Development of a balanced experimental-computational approach to understanding the mechanics of proximal femur fractures. *Med. Eng. Phys.* 36(6):793–799, 2014.
[24]Helgason, B., M. Viceconti, T. P. Runarsson, and S. Brynjolfsson. On the mechanical stability of porous coated press fit titanium implants: a finite element study of a pushout test. *J. Biomech.* 41:1675–1681, 2008.
[25]Jóhannesdóttir, F., T. Aspelund, J. Reeve, K. E. Poole, S. Sigurdsson, T. B. Harris, V. G. Gudnason, and G. Sigurdsson. Similarities and differences between sexes in regional loss of cortical and trabecular bone in the mid-femoral neck: the AGES-Reykjavik Longitudinal Study. *J. Bone Miner. Res.* 28:2165–2176, 2013.
[26]Jóhannesdottir, F., K. E. S. Poole, J. Reeve, K. Siggeirsdottir, T. Aspelund, B. Mogensen, B. Y. Jonsson, S. Sigurdsson, T. B. Harris, V. G. Gudnason, and G. Sigurdsson. Distribution of cortical bone in the femoral neck and hip fracture: a prospective case–control analysis of 143 incident hip fractures; the AGES-REYKJAVIK study. *Bone* 48:1268–1276, 2011.
[27]Johannesdottir, F., E. Thrall, J. Muller, T. M. Keaveny, D. L. Kopperdahl, and M. L. Bouxsein. Comparison of non-invasive assessments of strength of the proximal femur. *Bone* 105:93–102, 2017.
[28]Juszczyk, M. M., L. Cristofolini, M. Salva, L. Zani, E. Schileo, and M. Viceconti. Accurate in vitro identification of fracture onset in bones: failure mechanism of the proximal human femur. *J. Biomech.* 46:158–164, 2013.
[29]Keyak, J. H. Improved prediction of proximal femoral fracture load using nonlinear finite element models. *Med. Eng. Phys.* 23:165–173, 2001.
[30]Keyak, J. H., S. A. Rossi, K. A. Jones, and H. B. Skinner. Prediction of femoral fracture load using automated finite element modeling. *J. Biomech.* 31:125–133, 1998.
[31]Keyak, J. H., S. Sigurdsson, G. S. Karlsdottir, D. Oskarsdottir, A. Sigmarsdottir, J. Kornak, T. B. Harris, G. Sigurdsson, B. Y. Jonsson, K. Siggeirsdottir, G. Eiriksdottir, V. Gudnason, and T. F. Lang. Effect of finite element model loading condition on fracture risk assessment in men and women: the AGES-Reykjavik study. *Bone* 57:18–29, 2013.
[32]Kheirollahi, H., and Y. Luo. Identification of high stress and strain regions in proximal femur during single-leg stance and sideways fall using QCT-based finite element model. *Int. J. Med. Health Biomed. Bioeng. Pharm. Eng.* 9 (8):633–640, 2015.
[33]Kopperdahl, D. L., T. Aspelund, P. F. Hoffmann, S. Sigurdsson, K. Siggeirsdottir, T. B. Harris, V. Gudnason, and T. M. Keaveny. Assessment of incident spine and hip fractures in women and men using finite element analysis of CT scans. *J. Bone Miner. Res.* 29:570–580, 2014.

[34]Kopperdahl, D. L., and T. M. Keaveny. Yield strain behavior of trabecular bone. *J. Biomech.* 31:601–608, 1998.
[35]Lang, T. F., S. Sigurdsson, G. Karlsdottir, D. Oskarsdottir, A. Sigmarsdottir, J. Chengshi, J. Kornak, T. B. Harris, G. Sigurdsson, B. Y. Jonsson, K. Siggeirsdottir, G. Eiriksdottir, V. Gudnason, and J. H. Keyak. Age-related loss of proximal femoral strength in elderly men and women: the Age Gene/Environment Susceptibility Study-Reykjavik. *Bone* 50(3):743–748, 2012.
[36]Lotz, J. C., E. J. Cheal, and W. C. Hayes. Stress distributions within the proximal femur during gait and falls: implications for osteoporotic fracture. *Osteoporos. Int.* 5:252–261, 1995.
[37]Manske, S. L., T. Liu-Ambrose, D. M. L. Cooper, S. Kontulainen, P. Guy, B. B. Forster, and H. A. McKay. Cortical and trabecular bone in the femoral neck both contribute to proximal femur failure load prediction. *Osteoporos. Int.* 20:445–453, 2009.
[38]Mayhew, P. M., C. D. Thomas, J. G. Clement, N. Loveridge, T. J. Beck, W. Bonfield, C. J. Burgoyne, and J. Reeve. Relation between age, femoral neck cortical stability, and hip fracture risk. *Lancet* 366:129–135, 2005.
[39]Michelson, J. D., A. Myers, R. Jinnah, Q. Cox, and M. V. Natta. Epidemiology of hip fractures among the elderly. Risk factors for fracture type. *Clin. Orthop.* 311:129–135, 1995.
[40]Morgan, E. F., H. H. Bayraktar, and T. M. Keaveny. Trabecular bone modulus–density relationships depend on anatomic site. *J. Biomech.* 36:897–904, 2003.
[41]Nawathe, S., H. Akhlaghpour, L. M. Bouxsein, and T. M. Keaveny. Microstructural failure mechanisms in the human proximal femur for sideways fall loading. *J. Bone Miner. Res.* 29–2:507–515, 2014.
[42]Orwoll, E. S., L. M. Marshall, C. M. Nielson, S. R. Cummings, J. Lapidus, J. A. Cauley, K. Ensrud, N. Lane, P. R. Hoffmann, D. L. Kopperdahl, and T. M. Keaveny. Finite element analysis of the proximal femur and hip fracture risk in older men. *J. Bone Miner. Res.* 24:475–483, 2009.
[43]Parkkari, J., P. Kannus, M. Palvanen, A. Natri, J. Vainio, H. Aho, I. Vuori, and M. Järvinen. Majority of hip fractures occur as a result of a fall and impact on the greater trochanter of the femur: a prospective controlled hip fracture study with 206 consecutive patients. *Calcif. Tissue Int.* 65:183–187, 1999.
[44]Pulkkinen, P., J. Partanen, P. Jalovaara, and T. Jamsa. Combination of bone mineral density and upper femur geometry improves the prediction of hip fracture. *Osteoporos. Int.* 15:274–280, 2004.
[45]Schileo, E., L. Balistreri, L. Grassi, L. Cristofolini, and F. Taddei. To what extent can linear finite element models of human femora predict failure under stance and fall loading configurations? *J. Biomech.* 47:3531–3538, 2014.
[46]Schileo, E., F. Taddei, L. Cristofolini, and M. Viceconti. Subject-specific finite element models implementing a maximum principal strain criterion are able to estimate failure risk and fracture location on human femurs tested in vitro. *J. Biomech.* 41:356–367, 2008.
[47]Siris, E. S., Y. T. Chen, T. A. Abbott, E. Barrett-Connor, P. D. Miller, L. E. Wehren, and M. L. Berger. Bone mineral density thresholds for pharmacological intervention to prevent fractures. *Arch. Intern. Med.* 164:1108–1112, 2004.
[48]Stone, K. L., D. G. Seeley, L. Y. Lui, J. A. Cauley, K. Ensrud, W. S. Browner, M. C. Nevitt, and S. R. Cummings. BMD at multiple sites and risk of fracture of multiple types: long-term results from the Study of Osteoporotic Fractures. *J. Bone Miner. Res.* 18:1947–1954, 2003.
[49]Szulc, P. Bone density, geometry, and fracture in elderly men. *Curr. Osteoporos. Rep.* 4:57–63, 2006.
[50]Thomas, C. D., P. M. Mayhew, J. Power, K. E. Poole, L. Loveridge, J. G. Clement, C. L. Burgoyne, and J. Reeve. Femoral neck trabecular bone: loss with aging and role in preventing fracture. *J. Bone Miner. Res.* 24:1808–1818, 2009.
[51]Tinetti, M. E., M. Speechley, and S. F. Ginter. Risk factors for falls among elderly persons living in the community. *N. Engl. J. Med.* 319:1701–1707, 1988.
[52]Varga, P., J. Schwiedrzik, P. K. Zysset, L. Fliri-Hofmann, D. Widmer, B. Gueorguiev, M. Blauth, and M. Windolf. Nonlinear quasi-static finite element simulations predict in vitro strength of human proximal femora assessed in a dynamic sideways fall setup. *J. Mech. Behav. Biomed. Mater.* 57:116–127, 2016.
[53]Vaughn, D., M. Canning, and J. W. Hutchinson. Coupled plastic wave propagation and column buckling. *J. Appl. Mech.* 72:139–146, 2005.
[54]Verhulp, E., B. V. Rietbergen, and R. Huiskes. Load distribution in the healthy and osteoporotic human proximal femur during a fall to the side. *Bone* 42(1):30–35, 2008.
[55]Wainwright, S. A., L. M. Marshall, K. E. Ensrud, J. A. Cauley, D. M. Black, T. A. Hillier, M. C. Hochberg, M. T. Vogt, and E. S. Orwoll. Hip fracture in women without osteoporosis. *J. Clin. Endocrinol. Metab.* 90:2787–2793, 2005.
[56]Yu, J. L., X. Wang, Z. G. Wei, and E. H. Wang. Deformation and failure mechanism of dynamically loaded sandwich beams with aluminum foam core. *Int. J. Impact Eng* 28:331–347, 2003.